

Article

Inorganic Green Pigments Based on $\text{LaSr}_2\text{AlO}_5$

Kazuki Yamaguchi ¹, Akari Takemura ¹, Saki Furumoto ¹, Ryohei Oka ²  and Toshiyuki Masui ^{1,*}

¹ Department of Chemistry and Biotechnology, Faculty of Engineering, and Center for Research on Green Sustainable Chemistry, Tottori University, 4-101, Koyama-cho Minami, Tottori 680-8552, Japan; yamaguchi@tottori-u.ac.jp (K.Y.); m19j5023a@edu.tottori-u.ac.jp (A.T.); b19t3072m@gmail.com (S.F.)

² Field of Advanced Ceramics, Department of Life Science and Applied Chemistry, Nagoya Institute of Technology, Gokiso, Showa, Nagoya 466-8555, Japan; oka.ryohei@nitech.ac.jp

* Correspondence: masui@tottori-u.ac.jp; Tel.: +81-857-31-5264

Abstract: $\text{La}_{1.03}\text{Sr}_{1.97}\text{Al}_{0.97}\text{M}_{0.03}\text{O}_5$ ($M = \text{Fe}, \text{Co}, \text{Ni}, \text{and Cu}$) samples were synthesized using a citrate sol–gel method to develop a novel environmentally friendly inorganic green pigment. Among them, the Co-doped sample exhibited a vivid yellow, but not green. Then, $(\text{La}_{0.94}\text{Ca}_{0.06})\text{Sr}_2(\text{Al}_{0.97}\text{Mn}_{0.03})\text{O}_5$ was synthesized and characterized with respect to the crystal structure, optical properties, and color. The sample was obtained in a single-phase form and the lattice volume was smaller than that of the $(\text{La}_{0.94}\text{Ca}_{0.06})\text{Sr}_2\text{AlO}_5$ sample, indicating that Mn ions in the lattice of the sample were pentavalent. The sample exhibited optical absorption at a wavelength below 400 nm and around 650 nm. These absorptions were attributed to the ligand, the metal charge transfer (LMCT), and d-d transitions of Mn^{5+} . Because the green light corresponding to 500 to 560 nm was reflected strongly, the synthesized sample exhibited a bright green color. $(\text{La}_{0.94}\text{Ca}_{0.06})\text{Sr}_2(\text{Al}_{0.97}\text{Mn}_{0.03})\text{O}_5$ showed high brightness ($L^* = 50.1$) and greenness ($a^* = -20.8$), and these values were as high as those of the conventional green pigments such as chromium oxide and cobalt green. Therefore, the $(\text{La}_{0.94}\text{Ca}_{0.06})\text{Sr}_2(\text{Al}_{0.97}\text{Mn}_{0.03})\text{O}_5$ pigment is a potential candidate for a novel environmentally friendly inorganic green pigment.

Keywords: green pigment; environmentally friendly; Mn^{5+} ion; yellow pigment; Co^{2+} ion; lanthanum strontium aluminate



Citation: Yamaguchi, K.; Takemura, A.; Furumoto, S.; Oka, R.; Masui, T. Inorganic Green Pigments Based on $\text{LaSr}_2\text{AlO}_5$. *Ceramics* **2023**, *6*, 2269–2281. <https://doi.org/10.3390/ceramics6040138>

Academic Editor: Guillermo Monrós

Received: 29 September 2023
Revised: 25 October 2023
Accepted: 10 November 2023
Published: 22 November 2023



Copyright: © 2023 by the authors. Licensee MDPI, Basel, Switzerland. This article is an open access article distributed under the terms and conditions of the Creative Commons Attribution (CC BY) license (<https://creativecommons.org/licenses/by/4.0/>).

1. Introduction

Inorganic pigments are widely used as coloring materials for ceramics, glasses, plastics, and glazes because they have good thermal stabilities and resistances to climatic conditions. Among various colors, a greenish color makes us feel reposed, healed and relaxed; therefore, it has been used for a variety of applications. A characteristic of green is that it brings peaceful images of woods and forests. In addition, green signifies safety on traffic signs and public guideboards, and such feelings are widely accepted by people [1]. Thus, green is also used for information boards in evacuation centers and an emergency exits, etc. Moreover, because green is an intermediate color on the hue circle, it is used in various situations for harmonization with other colors.

Currently, chromium oxide (Cr_2O_3), chromium green, cobalt green ($\text{CoO}\cdot n\text{ZnO}$), and so on are used as commercially available inorganic green pigments. For Cr_2O_3 , studies have been conducted to improve its optical reflectance properties by mixing it with TiO_2 , Al_2O_3 , and V_2O_5 [2], or by substituting other metal ions at the Cr^{3+} site, as in $\text{Cr}_{2-x}\text{Al}_x\text{O}_3$ [3]. Sangeetha et al. found that Cr_2O_3 added with rare earth elements improved the greenness of the reflectance without decreasing the greenness [4]. Cr^{3+} is not a harmful ion but Cr_2O_3 has been synthesized by reducing the $\text{Na}_2\text{Cr}_2\text{O}_7$ or pyrolysis of CrO_3 , which contains Cr^{6+} [5]. Chromium green is composed of iron blue ($\text{Fe}_4[\text{Fe}(\text{CN})_6]_3$) and chrome yellow (PbCrO_4) and is used in paints because of its high hiding power. However, chrome yellow contains Pb and Cr^{6+} . Cr^{6+} is identified as a carcinogen by the International Agency for

Research on Cancer (IARC), and so is well known as a highly toxic element. At the same time, Pb is identified as possible carcinogenesis. On the other hand, the safety of CoO in cobalt green has also been questioned due to the concern about adverse effects on the human body. The use of these pigments has been restricted because they contain harmful elements (e.g., Cd, Pb, and Cr) and CoO, which has deleterious effect on the human body and the environment. Therefore, there is a strong desire to develop environmentally friendly inorganic green pigments to replace harmful inorganic pigments.

Based on this background, in order to develop novel environmentally friendly inorganic green pigments, we took note of pentavalent manganese (Mn^{5+}) ions as a coloring source. Mn ions are not only harmless but also inexpensive and exhibit various valences to be utilized in multiple applications. Mn^{5+} absorbs light with a wavelength of 400 nm or less based on ligand-to-metal charge transfer (LMCT) transition and d-d transition (${}^3\text{A}_2 \rightarrow {}^3\text{T}_1$ (${}^3\text{P}$)) [6,7]. Visible light around 650 nm is also absorbed by d-d transition attributed to ${}^3\text{A}_2 \rightarrow {}^3\text{T}_1$ (${}^3\text{F}$), and therefore, green coloration can be expected by using Mn^{5+} . Although Mn^{5+} ions tend to be generally unstable, they can be stable in the following situation: Mn ions are substituted in tetrahedral sites as well as a host compound, which is comprised of larger ionic radius elements such as alkali earth metal (Sr and Ba) and smaller ionic radius elements such as P and Al [6]. Actually, various Mn^{5+} -containing compounds have been reported [7–12] such as turquoise color pigments based on apatite-type $\text{Ba}_5\text{Mn}_{3-x}\text{M}_x\text{O}_{12}\text{Cl}$ ($\text{M} = \text{V}, \text{P}$) [13] and $\text{Ba}_3(\text{MO}_4)_2:\text{Mn}^{5+}$ ($\text{M} = \text{V}, \text{P}$) phosphors [14].

We focused on $\text{LaSr}_2\text{AlO}_5$ as a host material because it contains only low toxicity elements. $\text{LaSr}_2\text{AlO}_5$ adopts a tetragonal structure (space group: $I4/mcm$) [15]. This complex oxide is stacked alternately with an 8-coordinated $\text{La}^{3+}/\text{Sr}^{2+}$ layer, a 10-coordinated Sr^{2+} layer, and a 4-coordinated Al^{3+} layer through O^{2-} . A number of papers have also reported the use of $\text{LaSr}_2\text{AlO}_5$ as a base material for photocatalysts and phosphors [15–20]. There are many compounds in which La^{3+} is replaced by other elements, but few in which the Al^{3+} is replaced.

In this study, therefore, $\text{La}_{1.03}\text{Sr}_{1.97}\text{Al}_{0.97}\text{M}_{0.03}\text{O}_5$ ($\text{M} = \text{Fe}, \text{Co}, \text{Ni}, \text{and Cu}$) samples, whose Al^{3+} site was substituted by various transition metal elements, had their color properties characterized. Among them, the Co-doped sample exhibited a vivid yellow, but not green. Thus, $\text{La}_{1-2x}\text{Ca}_{2x}\text{Sr}_2\text{Al}_{1-x}\text{Mn}_x\text{O}_5$ ($x = 0$ and 0.03) samples were synthesized to obtain a new environmentally friendly green pigment. The Al^{3+} site in the $\text{LaSr}_2\text{AlO}_5$ host was partially substituted by Mn^{5+} ions. At the same time, the La^{3+} site was replaced by Ca^{2+} for charge compensation. The color properties of the samples were evaluated and compared with commercially available inorganic green pigments.

2. Materials and Methods

2.1. Synthesis

The $\text{LaSr}_2(\text{Al}_{0.97}\text{Fe}_{0.03})\text{O}_5$, $\text{La}_{1.03}\text{Sr}_{1.97}(\text{Al}_{0.97}\text{M}_{0.03})\text{O}_5$ ($\text{M}: \text{Ni}$ and Cu), and $\text{La}_{1+x}\text{Sr}_{2-x}(\text{Al}_{1-x}\text{Co}_x)\text{O}_5$ ($x = 0, 0.03, 0.05$ and 0.10) samples were synthesized using a citrate sol–gel method. $\text{La}(\text{NO}_3)_3 \cdot 6\text{H}_2\text{O}$ (FUJIFILM Wako Pure Chemical Industries Ltd., Osaka, Japan, 99.9%), $\text{Sr}(\text{NO}_3)_2$ (FUJIFILM Wako Pure Chemical Industries Ltd., 98.0%), $\text{Al}(\text{NO}_3)_3 \cdot 9\text{H}_2\text{O}$ (FUJIFILM Wako Pure Chemical Industries Ltd., 99.9%), $\text{Fe}(\text{NO}_3)_3 \cdot 9\text{H}_2\text{O}$ (FUJIFILM Wako Pure Chemical Industries Ltd., 99.9%), $\text{Co}(\text{NO}_3)_2 \cdot 6\text{H}_2\text{O}$ (FUJIFILM Wako Pure Chemical Industries Ltd., 99.5%), $\text{Cu}(\text{NO}_3)_2 \cdot 3\text{H}_2\text{O}$ (FUJIFILM Wako Pure Chemical Industries Ltd., 99.9%), and $\text{Ni}(\text{NO}_3)_2 \cdot 6\text{H}_2\text{O}$ (Kishida Chemical Co. Ltd., Osaka, Japan, 98.0%) were weighed so as to obtain the objective compositions and were dissolved in deionized water to adjust the La, Sr, and (Al + M) concentrations to 0.2 mol L^{-1} . After the solution was stirred homogeneously, citric acid (FUJIFILM Wako Pure Chemical Industries Ltd., 98.0%) was added as a chelating agent to complex the cations into the solution in the mole ratio 2:1 with regard to the total cations (La, Sr, Al, and M). The mixed solution was stirred at $80 \text{ }^\circ\text{C}$ until a gel was obtained. Then, the gel was heated in an oven at $120 \text{ }^\circ\text{C}$ for 24 h and completely dried at $350 \text{ }^\circ\text{C}$ on a mantle heater. The dried gel was calcined in an alumina crucible at $500 \text{ }^\circ\text{C}$ for 8 h in air. After the calcination, the sample was heated again in an

alumina boat at 1400 °C for 9 h in air. Before characterization, the sample was ground in an agate mortar with agate pestle.

$(\text{La}_{1-2x}\text{Ca}_{2x})\text{Sr}_2(\text{Al}_{1-x}\text{Mn}_x)\text{O}_5$ ($x = 0$ and 0.03) samples were prepared by the same procedure described above. The starting materials, $\text{La}(\text{NO}_3)_3 \cdot 6\text{H}_2\text{O}$, $\text{Ca}(\text{NO}_3)_2 \cdot 4\text{H}_2\text{O}$ (FUJIFILM Wako Pure Chemical Industries Ltd., 98.5%), $\text{Sr}(\text{NO}_3)_2$, $\text{Al}(\text{NO}_3)_3 \cdot 9\text{H}_2\text{O}$, and $(\text{CH}_3\text{COO})_2\text{Mn} \cdot 4\text{H}_2\text{O}$ (FUJIFILM Wako Pure Chemical Industries Ltd., 99.9%), were weighed stoichiometrically.

2.2. Characterization

X-ray powder diffraction (XRD) was conducted using an X-ray diffractometer (Rigaku Corporation, Tokyo, Japan Ultima IV) to identify the crystal phase and structure. The XRD patterns were taken with $\text{Cu-K}\alpha$ radiation operating with a tube voltage of 40 kV and a tube current of 40 mA. The data were collected by scanning over the 2θ range of 20–80°. The sampling width was 0.02° and the scan speed was 6° min^{-1} . The lattice volumes were calculated from the XRD peak angles refined by $\alpha\text{-Al}_2\text{O}_3$ as a standard and using the CellCalc Ver. 2.20 software. The Rietveld refinement of the resulting XRD patterns was performed by the RIETAN-FP software (version 3.12) package to determine the precise crystal structure [21]. From the Rietveld refinement, the following final R-factors were obtained: Rwp (R-weighted pattern), Rp (R-pattern), Re (R-expected), S (goodness-of-fit indicator), and RF (R-structure factor). The optical reflectance spectra of the as-prepared samples were recorded on an ultraviolet-visible (UV-Vis) spectrometer (JASCO Corporation, Tokyo, Japan, V-770 with an integrating sphere attachment) using a standard white plate as a reference. The step width was 1 nm and the scan rate was 1000 nm min^{-1} . The color properties of the powder samples were evaluated in terms of the Commission Internationale de l'Éclairage (CIE) $L^*a^*b^*Ch^\circ$ system using a colorimeter (Konica-Minolta, INC., Tokyo, Japan, CR-400). A standard C illuminant was used for the colorimetric measurements. The L^* parameter indicates the brightness or darkness in a neutral grayscale. The a^* values represent the red–green axes, and the b^* value yellow–blue axes. The chroma parameter (C) means the color saturation and is calculated with the formula, $C = [(a^*)^2 + (b^*)^2]^{1/2}$. The hue angle (h°) ranges from 0 to 360° and is calculated with the formula $h^\circ = \tan^{-1}(b^*/a^*)$. The standard deviations of all values for the $L^*a^*b^*Ch^\circ$ color coordinate data were less than 0.1.

3. Results and Discussion

3.1. $\text{La}_{1+x}\text{Sr}_{2-x}(\text{Al}_{1-x}\text{M}_x)\text{O}_5$ (M : Fe, Co, Ni, and Cu)

3.1.1. X-ray Powder Diffraction (XRD)

Figure 1 shows the XRD patterns of the $\text{LaSr}_2\text{AlO}_5$, $\text{LaSr}_2(\text{Al}_{0.97}\text{Fe}_{0.03})\text{O}_5$, and $\text{La}_{1.03}\text{Sr}_{1.97}(\text{Al}_{0.97}\text{M}_{0.03})\text{O}_5$ (M : Co, Ni, and Cu) samples. In the sample containing Fe, the objective $\text{LaSr}_2\text{AlO}_5$ phase was obtained in a single-phase form. On the other hand, in the samples containing Co, Ni, and Cu, the target $\text{LaSr}_2\text{AlO}_5$ phase was obtained as the main phase, but a few peaks of SrLaAlO_4 and SrLaNiO_4 were observed as impurities, resulting in a mixed phase.

3.1.2. Ultraviolet-Visible (UV-Vis) Reflectance Spectra

The UV-Vis reflectance spectra of $\text{LaSr}_2\text{AlO}_5$, $\text{LaSr}_2(\text{Al}_{0.97}\text{Fe}_{0.03})\text{O}_5$ and $\text{La}_{1.03}\text{Sr}_{1.97}(\text{Al}_{0.97}\text{M}_{0.03})\text{O}_5$ (M : Co, Ni, and Cu) are depicted in Figure 2. In the case of $M = \text{Fe}$, weak optical absorption due to the d-d transition of Fe^{3+} [22] was observed in the visible region around 420 nm. When M was Ni, the sample absorbed visible light around 650 nm because of the d-d transition of Ni^{2+} [23]. The sample with Cu absorbed visible light less than 400 nm and longer than 700 nm. These absorptions were attributed to the charge transfer between O_{2p} - Cu_{3d} orbitals and the d-d transition of Cu^{2+} [24]. In the sample with Co, visible light less than 450 nm was absorbed, which was based on the charge transfer transition between O_{2p} - Co_{3d} orbitals and the d-d transition of Co^{2+} [25,26]. In general, the energy gap of the d-d transition of Co^{2+} at the tetrahedral site corresponds to green–red light from 530 to 630 nm. In this study, the Al^{3+} site (ionic radius: 0.039 nm, 4-coordination [27]) was

substituted with Co^{2+} (ionic radius: 0.058 nm, 4-coordination [27]), resulting in a stronger crystal field surrounding Co^{2+} and the absorption of higher energy light around 450 nm, corresponding to the blue light region.

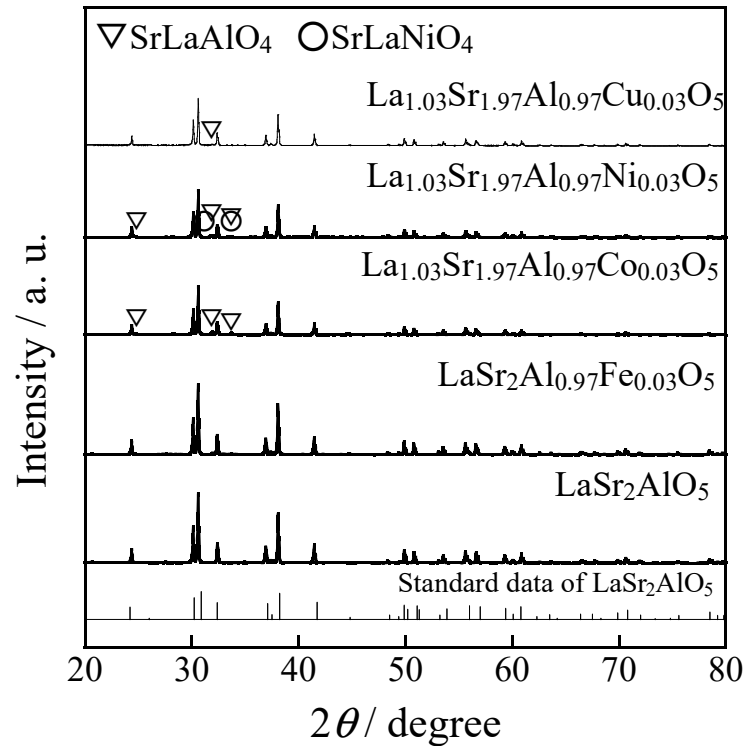


Figure 1. XRD patterns of the $\text{LaSr}_2\text{AlO}_5$, $\text{LaSr}_2(\text{Al}_{0.97}\text{Fe}_{0.03})\text{O}_5$, and $\text{La}_{1.03}\text{Sr}_{1.97}(\text{Al}_{0.97}\text{M}_{0.03})\text{O}_5$ (M : Co, Ni, and Cu) samples. The standard data of $\text{LaSr}_2\text{AlO}_5$ is based on the literature reported by Im, W.B et al. (2009) [15].

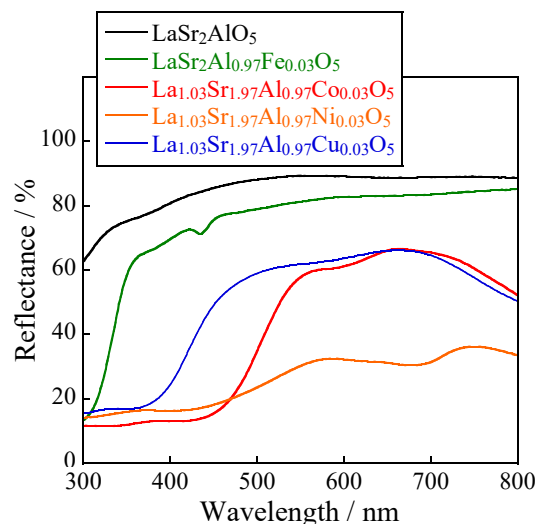


Figure 2. UV-Vis reflectance spectra for the $\text{LaSr}_2\text{AlO}_5$, $\text{LaSr}_2(\text{Al}_{0.97}\text{Fe}_{0.03})\text{O}_5$, and $\text{La}_{1.03}\text{Sr}_{1.97}(\text{Al}_{0.97}\text{M}_{0.03})\text{O}_5$ (M : Co, Ni, and Cu) samples.

3.1.3. Color Property

The $L^*a^*b^*Ch^\circ$ color coordinate data of the $\text{LaSr}_2\text{AlO}_5$, $\text{LaSr}_2(\text{Al}_{0.97}\text{Fe}_{0.03})\text{O}_5$, and $\text{La}_{1.03}\text{Sr}_{1.97}(\text{Al}_{0.97}\text{M}_{0.03})\text{O}_5$ (M : Co, Ni, and Cu) powder samples are summarized in Table 1. The sample photographs are also shown in Figure 3. The $\text{LaSr}_2\text{AlO}_5$ sample reflected the

entire visible light region and was white. For $M = \text{Fe}^{3+}$ and Cu^{2+} , the visible light region was almost completely reflected due to the weak d-d transition, and the samples were almost white. The sample with Ni^{2+} was a dingy green. This is due to the impurity phase of SrLaNiO_4 , which reduces the reflectance of visible light. In the case of Co^{2+} doping, a bright yellow color was obtained. In general, Co^{2+} ions exhibit a vivid blue color in tetrahedral coordination, as in cobalt blue (CoAl_2O_4) [28,29]. In the Co-doped sample in this study, Co^{2+} is also in a 4-coordinated environment. Despite this, interestingly, the sample exhibited a yellow color. This is a rare case.

Table 1. Color coordinates for the $\text{LaSr}_2\text{AlO}_5$, $\text{LaSr}_2(\text{Al}_{0.97}\text{Fe}_{0.03})\text{O}_5$, and $\text{La}_{1.03}\text{Sr}_{1.97}(\text{Al}_{0.97}\text{M}_{0.03})\text{O}_5$ (M : Co, Ni, and Cu) samples.

Samples	L^*	a^*	b^*	C	h°
$\text{LaSr}_2\text{AlO}_5$	96.7	−0.69	+2.84	2.92	—
$\text{LaSr}_2\text{Al}_{0.97}\text{Fe}_{0.03}\text{O}_5$	93.2	−0.24	+5.75	5.76	92.4
$\text{La}_{1.03}\text{Sr}_{1.97}\text{Al}_{0.97}\text{Co}_{0.03}\text{O}_5$	76.9	−4.36	+62.2	62.4	94.0
$\text{La}_{1.03}\text{Sr}_{1.97}\text{Al}_{0.97}\text{Ni}_{0.03}\text{O}_5$	55.6	−1.83	+25.7	25.8	94.1
$\text{La}_{1.03}\text{Sr}_{1.97}\text{Al}_{0.97}\text{Cu}_{0.03}\text{O}_5$	82.1	−2.45	+14.5	14.7	99.6

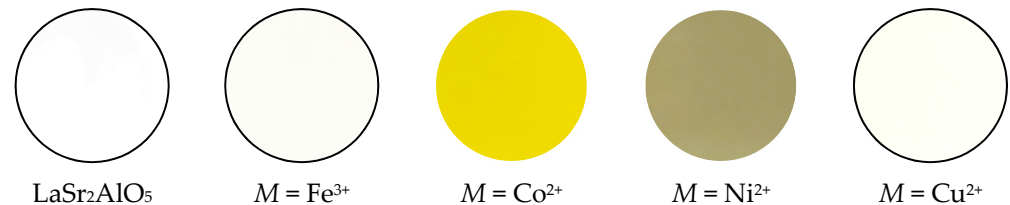


Figure 3. Photographs of the $\text{LaSr}_2\text{AlO}_5$, $\text{LaSr}_2(\text{Al}_{0.97}\text{Fe}_{0.03})\text{O}_5$, and $\text{La}_{1.03}\text{Sr}_{1.97}(\text{Al}_{0.97}\text{M}_{0.03})\text{O}_5$ (M : Co, Ni, and Cu) samples.

To investigate the composition dependence of the yellow-colored Co-doped samples, $\text{La}_{1+x}\text{Sr}_{2-x}(\text{Al}_{1-x}\text{Co}_x)\text{O}_5$ ($x = 0.03, 0.05, \text{ and } 0.10$) samples were synthesized. X-ray powder diffraction measurements showed that the samples with $x = 0.05$ and 0.10 were mixed phases, as was the sample with $x = 0.03$, but the target $\text{LaSr}_2\text{AlO}_5$ phase was obtained as the main phase. The Co^{2+} content dependence on the lattice volume of the samples is summarized in Table 2. Since the ionic radius of Co^{2+} (0.090 nm, 8-coordination [27]) is smaller than that of Sr^{2+} (0.126 nm, 8-coordination [27])/ La^{3+} (0.116 nm, 8-coordination [27]), the lattice volume should shrink when the 8-coordination Sr(1)/La sites in the host material are replaced with Co^{2+} . However, the lattice volume of the sample increased with Co^{2+} content up to $x = 0.05$. As noted above, this indicates that the Al^{3+} sites in the host lattice were partially replaced by larger Co^{2+} ions. Therefore, the chromophore in this sample is considered to be a 4-coordinated Co^{2+} ion.

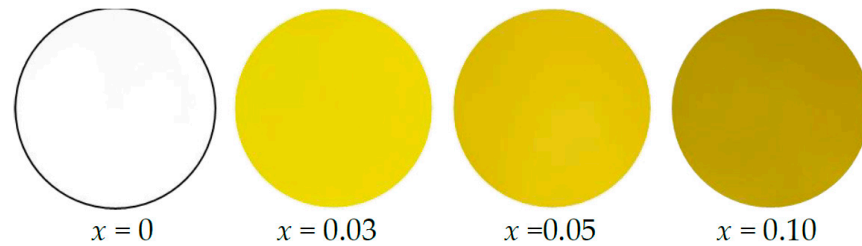
Table 2. Lattice volumes of the $\text{La}_{1+x}\text{Sr}_{2-x}(\text{Al}_{1-x}\text{Co}_x)\text{O}_5$ ($0 \leq x \leq 0.10$) samples. The numbers in parentheses are the estimated standard deviations.

x	Lattice Volume/nm ³
0	0.52431(6)
0.03	0.52486(4)
0.05	0.52538(4)
0.10	0.52541(6)

Table 3 summarizes the $L^*a^*b^*Ch^\circ$ color coordinate data for $\text{La}_{1+x}\text{Sr}_{2-x}(\text{Al}_{1-x}\text{Co}_x)\text{O}_5$ ($x = 0, 0.03, 0.05, \text{ and } 0.10$). The sample photographs are also shown in Figure 4. All samples exhibited a yellow color but become slightly darker with increasing Co^{2+} concentration.

Table 3. Color coordinate data for the $\text{La}_{1+x}\text{Sr}_{2-x}(\text{Al}_{1-x}\text{Co}_x)\text{O}_5$ ($x = 0, 0.03, 0.05, \text{ and } 0.10$) samples.

x	L^*	a^*	b^*	C	h°
0	96.7	−0.69	+2.84	2.92	–
0.03	76.9	−4.36	+62.2	62.4	94.0
0.05	75.8	−4.52	+67.2	67.4	93.8
0.10	62.2	−1.78	+58.7	58.7	91.7

**Figure 4.** Photographs of the $\text{La}_{1+x}\text{Sr}_{2-x}(\text{Al}_{1-x}\text{Co}_x)\text{O}_5$ ($x = 0, 0.03, 0.05, \text{ and } 0.10$) samples.

Unfortunately, the $\text{LaSr}_2(\text{Al}_{0.97}\text{Fe}_{0.03})\text{O}_5$ and $\text{La}_{1.03}\text{Sr}_{1.97}(\text{Al}_{0.97}\text{M}_{0.03})\text{O}_5$ (M : Co, Ni, and Cu) samples did not exhibit a green color, so we synthesized $(\text{La}_{1-2x}\text{Ca}_{2x})\text{Sr}_2(\text{Al}_{1-x}\text{Mn}_x)\text{O}_5$ ($x = 0, 0.03$) and characterized it in the next section.

3.2. $(\text{La}_{1-2x}\text{Ca}_{2x})\text{Sr}_2(\text{Al}_{1-x}\text{Mn}_x)\text{O}_5$ ($x = 0$ and 0.03)

3.2.1. X-ray Powder Diffraction (XRD)

Figure 5 shows the XRD patterns of the $(\text{La}_{1-2x}\text{Ca}_{2x})\text{Sr}_2(\text{Al}_{1-x}\text{Mn}_x)\text{O}_5$ ($x = 0$ and 0.03) and $(\text{La}_{0.94}\text{Ca}_{0.06})\text{Sr}_2\text{AlO}_{4.97}$ samples. All samples were obtained in a single-phase form. The lattice volume of each sample was calculated from the XRD peak angles and is summarized in Table 4. The lattice volume decreased in the order of undoped $> \text{Ca}^{2+}$ -doped $> \text{Ca}^{2+}$ - Mn^{5+} co-doped. In $(\text{La}_{0.94}\text{Ca}_{0.06})\text{Sr}_2\text{AlO}_{4.97}$, some of the La^{3+} (ionic radius: 0.116 nm, 8-coordination [27]) ions in $\text{LaSr}_2\text{AlO}_5$ were replaced by smaller Ca^{2+} ions (ionic radius: 0.112 nm, 8-coordination [27]), which resulted in the lattice volume contraction. In the sample co-doped with Ca^{2+} and Mn^{5+} , the lattice volume was further decreased. The ionic radii of the 4-coordinated Mn^{2+} and Mn^{4+} are 0.039 and 0.066 nm, respectively [27], and those are equal to or larger than Al^{3+} (ionic radius: 0.039 nm, 4-coordination [27]), so the lattice volume in Table 4 should be the same or increase when Mn^{2+} or Mn^{4+} is dissolved in the Al^{3+} site, but it actually decreased. Accordingly, the decrease in lattice volume was not only because La^{3+} was substituted with Ca^{2+} , but also because some of the Al^{3+} ions in the host material were replaced by smaller Mn^{5+} ions (ionic radius: 0.033 nm, 4-coordination [27]), although the substitution by Mn^{6+} is also in accordance with this result.

Table 4. Lattice volume of the $\text{LaSr}_2\text{AlO}_5$, $(\text{La}_{0.94}\text{Ca}_{0.06})\text{Sr}_2\text{AlO}_{4.97}$, and $(\text{La}_{0.94}\text{Ca}_{0.06})\text{Sr}_2(\text{Al}_{0.97}\text{Mn}_{0.03})\text{O}_5$ samples. The numbers in parentheses are the estimated standard deviations.

Samples	Lattice Volume/nm ³
$\text{LaSr}_2\text{AlO}_5$	0.52475(2)
$(\text{La}_{0.94}\text{Ca}_{0.06})\text{Sr}_2\text{AlO}_{4.97}$	0.52394(4)
$(\text{La}_{0.94}\text{Ca}_{0.06})\text{Sr}_2(\text{Al}_{0.97}\text{Mn}_{0.03})\text{O}_5$	0.52380(4)

The Rietveld analysis of the XRD patterns of $\text{LaSr}_2\text{AlO}_5$, $(\text{La}_{0.94}\text{Ca}_{0.06})\text{Sr}_2\text{AlO}_{4.97}$, and $(\text{La}_{0.94}\text{Ca}_{0.06})\text{Sr}_2(\text{Al}_{0.97}\text{Mn}_{0.03})\text{O}_5$ was performed to determine the average La–O, Sr–O, and Al–O bond length. The Rietveld refinement profiles of the samples are shown in Figure 6. The detailed crystallographic data are summarized in Table 5. The refined structural parameters of the samples are tabulated in Table 6. The crystallographic parameters of $\text{LaSr}_2\text{AlO}_5$ reported by W. B. Im et al. [15] were employed as the initial structure

for fitting. The refined crystal structure of $(\text{La}_{0.94}\text{Ca}_{0.06})\text{Sr}_2(\text{Al}_{0.97}\text{Mn}_{0.03})\text{O}_5$ illustrated by the VESTA program [30] is shown in Figure 7, where the Ca^{2+} and Mn^{5+} cations in $(\text{La}_{0.94}\text{Ca}_{0.06})\text{Sr}_2(\text{Al}_{0.97}\text{Mn}_{0.03})\text{O}_5$ were located at octahedral and tetrahedral sites, respectively. The average bond lengths of La–O, Sr(2)–O, and Al–O for the $\text{LaSr}_2\text{AlO}_5$, $(\text{La}_{0.94}\text{Ca}_{0.06})\text{Sr}_2\text{AlO}_{4.97}$, and $(\text{La}_{0.94}\text{Ca}_{0.06})\text{Sr}_2(\text{Al}_{0.97}\text{Mn}_{0.03})\text{O}_5$ samples are summarized in Table 7. In the case of $(\text{La}_{0.94}\text{Ca}_{0.06})\text{Sr}_2\text{AlO}_{4.97}$, the average Al–O bond length was longer than in $\text{LaSr}_2\text{AlO}_5$. This is because some of the La^{3+} (ionic radius: 0.116 nm, 8-coordination [27]) sites in $\text{LaSr}_2\text{AlO}_5$ were replaced by smaller Ca^{2+} ions (ionic radius: 0.112 nm, 8-coordination [27]), resulting in a shorter average La–O bond length. On the other hand, the average Al–O bond length of the $(\text{La}_{0.94}\text{Ca}_{0.06})\text{Sr}_2(\text{Al}_{0.97}\text{Mn}_{0.03})\text{O}_5$ sample was shorter than that of the $(\text{La}_{0.94}\text{Ca}_{0.06})\text{Sr}_2\text{AlO}_{4.97}$ sample. This is considered to be because some of the Al^{3+} ions (ionic radius: 0.039 nm, 4-coordination [27]) in $(\text{La}_{0.94}\text{Ca}_{0.06})\text{Sr}_2\text{AlO}_{4.97}$ were replaced by smaller Mn^{5+} (ionic radius: 0.033 nm, 4-coordination [27]) ions, resulting in shorter average Al–O bond length. Consequently, Mn ions are present as Mn^{5+} in the lattice of the $(\text{La}_{0.94}\text{Ca}_{0.06})\text{Sr}_2(\text{Al}_{0.97}\text{Mn}_{0.03})\text{O}_5$ sample.

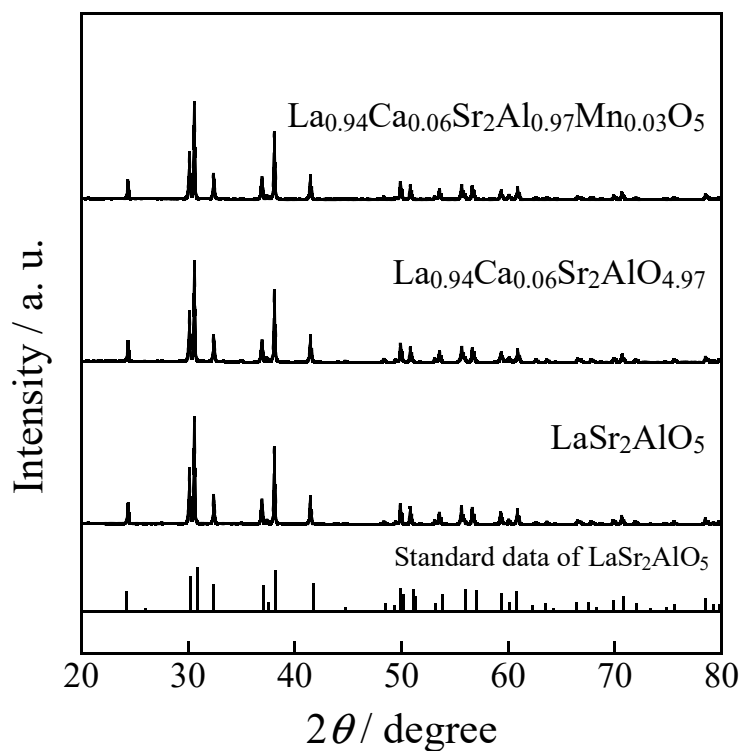


Figure 5. XRD patterns of the $(\text{La}_{1-2x}\text{Ca}_{2x})\text{Sr}_2(\text{Al}_{1-x}\text{Mn}_x)\text{O}_5$ ($x = 0$ and 0.03) and $(\text{La}_{0.94}\text{Ca}_{0.06})\text{Sr}_2\text{AlO}_{4.97}$ samples. The standard data of $\text{LaSr}_2\text{AlO}_5$ is based on the literature reported by Im, W.B et al. (2009) [15].

Table 5. Crystallographic data for the $\text{LaSr}_2\text{AlO}_5$, $(\text{La}_{0.94}\text{Ca}_{0.06})\text{Sr}_2\text{AlO}_{4.97}$, and $(\text{La}_{0.94}\text{Ca}_{0.06})\text{Sr}_2(\text{Al}_{0.97}\text{Mn}_{0.03})\text{O}_5$ samples refined via the Rietveld analysis. The numbers in parentheses are the estimated standard deviations.

Samples	$\text{LaSr}_2\text{AlO}_5$	$(\text{La}_{0.94}\text{Ca}_{0.06})\text{Sr}_2\text{AlO}_{4.97}$	$(\text{La}_{0.94}\text{Ca}_{0.06})\text{Sr}_2(\text{Al}_{0.97}\text{Mn}_{0.03})\text{O}_5$
Crystal system	Tetragonal	Tetragonal	Tetragonal
a/nm	0.688766(5)	0.688455(5)	0.688338(7)
b/nm	—	—	—
c/nm	1.105570(10)	1.105399(11)	1.105249(14)
V/nm^3	0.524481(7)	0.523926(8)	0.523677(10)
R_{wp}	4.391	4.684	3.647

Table 5. Cont.

Samples	$\text{LaSr}_2\text{AlO}_5$	$(\text{La}_{0.94}\text{Ca}_{0.06})\text{Sr}_2\text{AlO}_{4.97}$	$(\text{La}_{0.94}\text{Ca}_{0.06})\text{Sr}_2(\text{Al}_{0.97}\text{Mn}_{0.03})\text{O}_5$
R_p	2.943	3.122	2.372
R_e	2.663	2.637	2.537
S	1.649	1.776	1.437
R_F	2.403	2.556	2.465

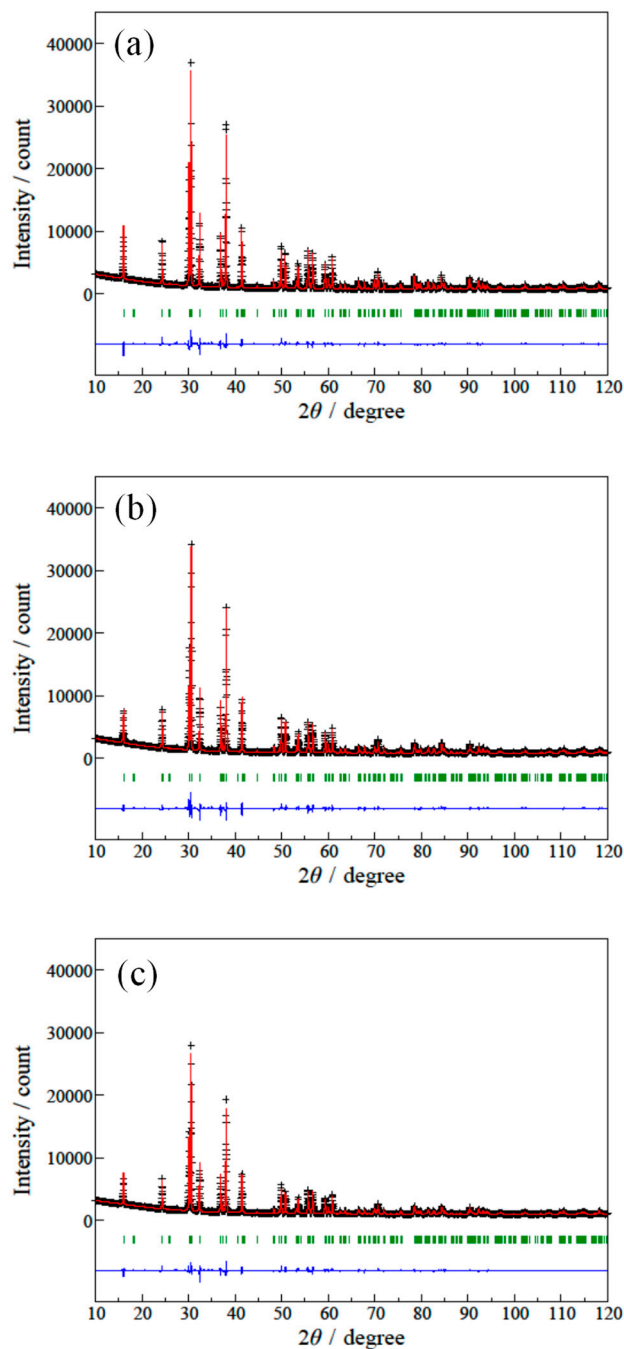


Figure 6. Rietveld refinement profiles of the XRD patterns for the (a) $\text{LaSr}_2\text{AlO}_5$, (b) $(\text{La}_{0.94}\text{Ca}_{0.06})\text{Sr}_2\text{AlO}_{4.97}$, and (c) $(\text{La}_{0.94}\text{Ca}_{0.06})\text{Sr}_2(\text{Al}_{0.97}\text{Mn}_{0.03})\text{O}_5$ samples. The black cross symbols and the solid red lines represent the observed and calculated intensities, respectively. The difference profiles between the observed and calculated patterns are depicted as a blue line at the bottom. The green vertical bars show the Bragg reflection peaks.

Table 6. Atomic coordinates and isotropic displacement factors (B_{iso}) for the $LaSr_2AlO_5$, $(La_{0.94}Ca_{0.06})Sr_2AlO_{4.97}$, and $(La_{0.94}Ca_{0.06})Sr_2(Al_{0.97}Mn_{0.03})O_5$ samples refined via the Rietveld analysis. The numbers in parentheses are the estimated standard deviations.

Atom	Site	Occupancy	x	y	z	$100 \times B_{iso}/nm^2$
$LaSr_2AlO_5$						
La	8h	0.5	0.31923(9)	=x(La) + 1/2	0	0.48(2)
Sr1	8h	0.5	=x(La)	=y(La)	0	= B_{iso} (La)
Sr2	4a	1	0	0	1/4	0.37(3)
Al	4b	1	1/2	0	1/4	0.39(9)
O1	4c	1	0	0	0	3.7(3)
O2	16l	1	0.1352(5)	=x(O2) + 1/2	0.1510(3)	0.97(10)
$(La_{0.94}Ca_{0.06})Sr_2AlO_{4.97}$^a						
La	8h	0.438(3)	0.3199(1)	=x(La) + 1/2	0	–
Ca	8h	0.062 ^b	=x(La)	=y(La)	0	–
Sr1	8h	0.5	=x(La)	=y(La)	0	–
Sr2	4a	1	0	0	1/4	–
Al	4b	1	1/2	0	1/4	–
O1	4c	0.893(14)	0	0	0	–
O2	16l	1	0.1343(5)	=x(O2) + 1/2	0.1488(3)	–
$(La_{0.94}Ca_{0.06})Sr_2(Al_{0.97}Mn_{0.03})O_5$^a						
La	8h	0.414(3)	0.3195(1)	0.8195	0	–
Ca	8h	0.086 ^b	=x(La)	=y(La)	0	–
Sr1	8h	0.5	=x(La)	=y(La)	0	–
Sr2	4a	1	0	0	1/4	–
Al	4b	0.973(10)	1/2	0	1/4	–
Mn	4b	0.027 ^c	1/2	0	1/4	–
O1	4c	1	0	0	0	–
O2	16l	1	0.1344(5)	=x(O2) + 1/2	0.1495(3)	–

^a The isotropic displacement parameters (B_{iso}) for the $(La_{0.94}Ca_{0.06})Sr_2AlO_{4.97}$ and $(La_{0.94}Ca_{0.06})Sr_2(Al_{0.97}Mn_{0.03})O_5$ samples were fixed with $LaSr_2AlO_5$. ^b (Ca, g) = 0.5 – (La, g). ^c (Mn, g) = 1.0 – (Al, g).

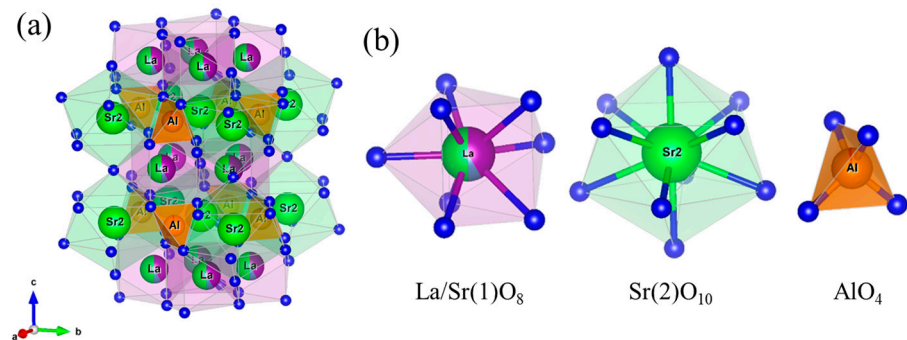


Figure 7. (a) Crystal structure obtained via the Rietveld analysis for $(La_{0.94}Ca_{0.06})Sr_2(Al_{0.97}Mn_{0.03})O_5$. (b) The octahedral coordination environment of $La/Sr(1)O_8$, the decahedral coordination environment of $Sr(2)O_{10}$, and the tetrahedral coordination environment of AlO_4 .

Table 7. Average bond length of La–O, Sr(2)–O, and Al–O for the $(La_{0.94}Ca_{0.06})Sr_2(Al_{0.97}Mn_{0.03})O_5$ sample refined via the Rietveld analysis.

Samples	$LaSr_2AlO_5$	$(La_{0.94}Ca_{0.06})Sr_2AlO_{4.97}$	$(La_{0.94}Ca_{0.06})Sr_2(Al_{0.97}Mn_{0.03})O_5$
La–O/nm	0.2625	0.2611	0.2615
Sr(2)–O/nm	0.3585	0.3597	0.3593
Al–O/nm	0.1712	0.1721	0.1716

3.2.2. Ultraviolet-Visible (UV-Vis) Reflectance Spectra

Figure 8 shows the UV-Vis reflectance spectra of the $LaSr_2AlO_5$, $(La_{0.94}Ca_{0.06})Sr_2AlO_{4.97}$, and $(La_{0.94}Ca_{0.06})Sr_2(Al_{0.97}Mn_{0.03})O_5$ samples. The results confirm the presence of Mn^{5+} ions in the co-doped sample. The samples without Mn^{5+} reflected totally visible light to exhibit a white color. On the other hand, the Mn^{5+} -doped sample strongly absorbed the light at wavelengths below 400 nm and around 650 nm. The former absorption was assigned to the combination of LMCT transition and the d-d transition attributed to the 3A_2 to 3T_1 (3P) transition of Mn^{5+} [6,7]. The latter was attributed to the d-d transition corresponding to the

3A_2 to 3T_1 (3F) transition of Mn^{5+} [6,7]. As a result, the $(La_{0.94}Ca_{0.06})Sr_2(Al_{0.97}Mn_{0.03})O_5$ sample only reflected light around 520 nm corresponding to green light, and showed a green color. If Mn ions are hexavalent, optical absorption based on Mn^{6+} ions appears at wavelengths below 450 nm and around 550 nm, due to the LMCT transition as well as the 2E_1 to 2T_1 transition of Mn^{6+} [6]. In that case, the sample should show an indigo color, not green. These crystallographic and optical reflectance properties support the fact that Mn ions are present not as Mn^{6+} but Mn^{5+} in the sample.

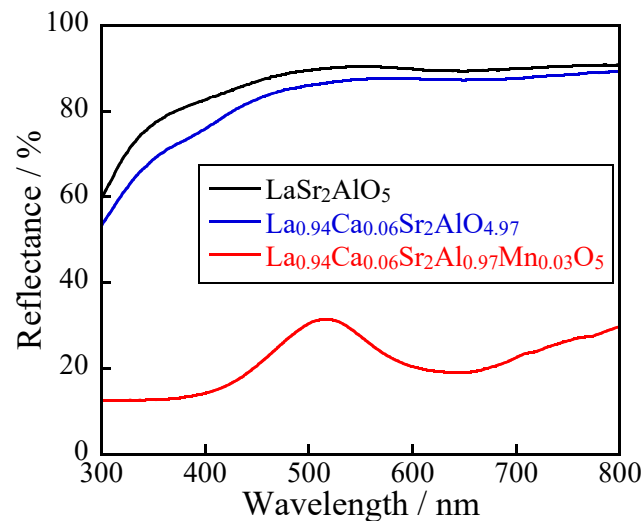


Figure 8. UV-Vis reflectance spectra for the $LaSr_2AlO_5$, $(La_{0.94}Ca_{0.06})Sr_2AlO_{4.97}$, and $(La_{0.94}Ca_{0.06})Sr_2(Al_{0.97}Mn_{0.03})O_5$ samples.

3.2.3. Color Properties

The $L^*a^*b^*Ch^\circ$ color coordinate data for the $LaSr_2AlO_5$, $(La_{0.94}Ca_{0.06})Sr_2AlO_{4.97}$, and $(La_{0.94}Ca_{0.06})Sr_2(Al_{0.97}Mn_{0.03})O_5$ pigments are summarized in Table 8. The photographs are also displayed in Figure 9. As discussed for the UV-Vis reflectance spectra in Figure 8, the samples without Mn^{5+} exhibited a white color due to the total reflection of visible light. For the $(La_{0.94}Ca_{0.06})Sr_2(Al_{0.97}Mn_{0.03})O_5$ pigment, a bright green color with a high L^* value (50.1) and a negatively high a^* value (-20.8) was achieved because the sample intensely reflected green light around 500–560 nm.

Table 8. Color coordinate data for the $LaSr_2AlO_5$, $(La_{0.94}Ca_{0.06})Sr_2AlO_{4.97}$, and $(La_{0.94}Ca_{0.06})Sr_2(Al_{0.97}Mn_{0.03})O_5$ pigments.

Sample	L^*	a^*	b^*	C	h°
$LaSr_2AlO_5$	96.2	-0.732	$+1.89$	2.03	111
$(La_{0.94}Ca_{0.06})Sr_2AlO_{4.97}$	95.5	-0.854	$+3.27$	3.38	104
$(La_{0.94}Ca_{0.06})Sr_2(Al_{0.97}Mn_{0.03})O_5$	50.1	-20.8	$+7.65$	22.2	160

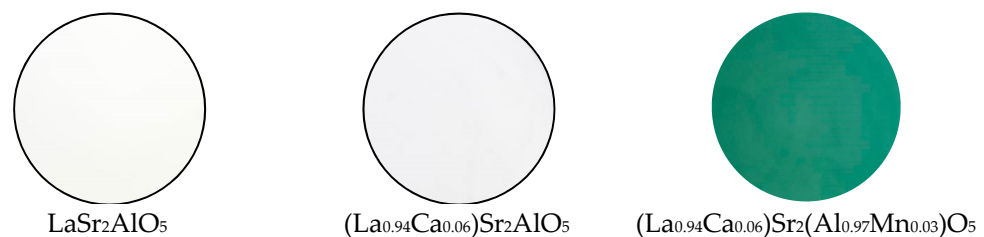


Figure 9. Photographs of the pellets of $LaSr_2AlO_5$, $(La_{0.94}Ca_{0.06})Sr_2AlO_{4.97}$, and $(La_{0.94}Ca_{0.06})Sr_2(Al_{0.97}Mn_{0.03})O_5$ powders.

3.2.4. Comparison with Commercially Available Pigments

The color parameters of the $(\text{La}_{0.94}\text{Ca}_{0.06})\text{Sr}_2(\text{Al}_{0.97}\text{Mn}_{0.03})\text{O}_5$ sample were compared with those of the commercial green pigments such as chromium green (Cr_2O_3) and cobalt green deep and pale ($\text{CoO}\cdot\text{ZnO}$), as listed in Table 9. Their photographs are also shown in Figure 10. The absolute value of a^* of the $(\text{La}_{0.94}\text{Ca}_{0.06})\text{Sr}_2(\text{Al}_{0.97}\text{Mn}_{0.03})\text{O}_5$ pigment was as high as those of the commercial pigments. The b^* of the synthesized pigment was positive and low, so its hue angle (h°) was 160° , close to 180° , which means the purest green color. Chromium oxide had negative high a^* and positive high b^* values, giving it a yellowish green color. Although the h° of cobalt green deep was the most ideal, its brightness (L^*) was lower than those of the other pigments, giving it a dark green color. Cobalt green pale had a higher absolute value of a^* but a negative b^* value, giving it a bluish green color. These results indicate that the color property of the $(\text{La}_{0.94}\text{Ca}_{0.06})\text{Sr}_2(\text{Al}_{0.97}\text{Mn}_{0.03})\text{O}_5$ pigment is well balanced for an environmentally friendly inorganic green pigment.

Table 9. Color coordinate data for the $(\text{La}_{0.94}\text{Ca}_{0.06})\text{Sr}_2(\text{Al}_{0.97}\text{Mn}_{0.03})\text{O}_5$ sample and the commercially available green pigments.

Sample	L^*	a^*	b^*	C	h°
$(\text{La}_{0.94}\text{Ca}_{0.06})\text{Sr}_2(\text{Al}_{0.97}\text{Mn}_{0.03})\text{O}_5$	50.1	−20.8	+7.65	22.2	160
Chromium oxide	50.2	−20.5	+18.2	27.4	138
Cobalt green deep	33.3	−19.9	+3.88	20.3	169
Cobalt green pale	52.3	−24.4	−5.53	25.0	193



Figure 10. Photographs of the pellets of $(\text{La}_{0.94}\text{Ca}_{0.06})\text{Sr}_2(\text{Al}_{0.97}\text{Mn}_{0.03})\text{O}_5$, chromium oxide, cobalt green deep, and cobalt green pale powders.

4. Conclusions

The $(\text{La}_{0.94}\text{Ca}_{0.06})\text{Sr}_2(\text{Al}_{0.97}\text{Mn}_{0.03})\text{O}_5$ sample was synthesized as an environmentally friendly inorganic green pigment. The sample was obtained in a single-phase form and the lattice volume was reduced compared with those of $\text{LaSr}_2\text{AlO}_5$ and $(\text{La}_{0.94}\text{Ca}_{0.06})\text{Sr}_2\text{AlO}_{4.97}$. These results indicate that a solid solution was successfully obtained, and Mn ions are present in the lattice as Mn^{5+} . The $(\text{La}_{0.94}\text{Ca}_{0.06})\text{Sr}_2(\text{Al}_{0.97}\text{Mn}_{0.03})\text{O}_5$ sample exhibited optical absorption in visible light at wavelengths below 400 nm and around 650 nm due to the LMCT and d-d transitions of Mn^{5+} . Therefore, this sample strongly reflected green light between 500 and 560 nm, and showed a bright green color. $(\text{La}_{0.94}\text{Ca}_{0.06})\text{Sr}_2(\text{Al}_{0.97}\text{Mn}_{0.03})\text{O}_5$ exhibited negatively high a^* (−20.8) and h° (160), which were comparable to those of the conventional green pigments containing toxic elements. In conclusion, $(\text{La}_{0.94}\text{Ca}_{0.06})\text{Sr}_2(\text{Al}_{0.97}\text{Mn}_{0.03})\text{O}_5$ could be a novel environmentally friendly inorganic green pigment.

Author Contributions: The following are the author contributions to this study: conceptualization, R.O. and T.M.; methodology, K.Y., R.O. and T.M.; validation, K.Y., R.O. and T.M.; investigation, K.Y., A.T., S.F. and R.O.; data curation, K.Y., A.T., S.F., R.O. and T.M.; writing—original draft preparation, K.Y.; writing—review and editing, T.M.; supervision, T.M.; funding acquisition, T.M. All authors have read and agreed to the published version of the manuscript.

Funding: This research was funded by JSPS KAKENHI, grant numbers JP22K04698 and JP20H02439.

Institutional Review Board Statement: Not applicable.

Informed Consent Statement: Not applicable.

Data Availability Statement: Data are contained within the article.

Conflicts of Interest: The authors declare no conflict of interest.

References

1. Valdez, P.; Mehrabian, A. Effects of Color on Emotions. *J. Exp. Psychol.-Gen.* **1994**, *123*, 394–409. [[CrossRef](#)]
2. Thongkanluang, T.; Kittiauchawal, T.; Limsuwan, P. Preparation and Characterization of Cr₂O₃-TiO₂-Al₂O₃-V₂O₅ Green Pigment. *Ceram. Int.* **2011**, *37*, 543–548. [[CrossRef](#)]
3. Muñoz, R.; Masó, N.; Julián, B.; Márquez, F.; Beltrán, H.; Escribano, P.; Cordoncillo, E. Environmental Study of Cr₂O₃-Al₂O₃ Green Ceramic Pigment Synthesis. *J. Eur. Ceram. Soc.* **2004**, *24*, 2087–2094. [[CrossRef](#)]
4. Sangeetha, S.; Basha, R.; Sreeram, K.J.; Sangilimuthu, S.N.; Unni Nair, B. Functional Pigments from Chromium(III) Oxide Nanoparticles. *Dyes Pigment.* **2012**, *94*, 548–552. [[CrossRef](#)]
5. Zhang, Y.; Li, Z.-H.; Qi, T.; Zheng, S.-L.; Li, H.-Q.; Xu, H.-B. Green Manufacturing Process of Chromium Compounds. *Environ. Prog.* **2005**, *24*, 44–50. [[CrossRef](#)]
6. Cao, R.; Qiu, J.; Yu, X.; Sun, X. Spectroscopic Investigation on BaSO₄: (Mn⁶⁺, Mn⁵⁺) Crystal. *ECS J. Solid State Sci. Technol.* **2013**, *2*, R237–R240. [[CrossRef](#)]
7. Dardenne, K.; Vivien, D.; Huguenin, D. Color of Mn(V)-Substituted Apatites A₁₀((B, Mn)O₄)₆F₂, A=Ba, Sr, Ca; B=P, VJ. *Solid State Chem.* **1999**, *146*, 464–472. [[CrossRef](#)]
8. Han, Y.; Ye, X.; Zhu, H.; Li, Y.; Kuang, X. New Oxygen-Deficient Cationic-Ordered Perovskites Containing Turquoise-Coloring Mn⁵⁺O₄ Tetrahedral Layers. *J. Solid State Chem.* **2017**, *247*, 20–23. [[CrossRef](#)]
9. Gschwend, P.M.; Niedbalka, D.; Gerken, L.R.H.; Herrmann, I.K.; Pratsinis, S.E. Simultaneous Nanothermometry and Deep-Tissue Imaging. *Adv. Sci.* **2020**, *7*, 2000370. [[CrossRef](#)]
10. Zheng, W.-C.; Wu, X.-X.; Fan, Y.-J. Studies of EPR Parameters for Mn⁵⁺-Doped Li₃PO₄ and Li₃VO₄ Crystals. *Spectrochim. Acta A* **2007**, *66*, 102–105.
11. Laha, S.; Tamilarasan, S.; Natarajan, S.; Gopalakrishnan, J. Stabilization of a Tetrahedral (Mn⁵⁺O₄) Chromophore in Ternary Barium Oxides as a Strategy toward Development of New Turquoise/Green-Colored Pigments. *Inorg. Chem.* **2016**, *55*, 3508–3514. [[CrossRef](#)]
12. Herren, M.; Riedener, T.; Güdel, H.U.; Albrecht, C.; Kaschuba, U.; Reinen, D. Near-Infrared Luminescence of Manganate(V)-Doped Phosphates and Vanadates. *J. Lumin.* **1992**, *53*, 452–456. [[CrossRef](#)]
13. Medina, E.A.; Li, J.; Stalick, J.K.; Subramanian, M.A. Intense Turquoise Colors of Apatite-Type Compounds with Mn⁵⁺ in Tetrahedral Coordination. *Solid State Sci.* **2016**, *52*, 97–105. [[CrossRef](#)]
14. Zhang, X.; Li, Y.; Hu, Z.; Chen, Z.; Qiu, J. A General Strategy for Controllable Synthesis of Ba₃(MO₄)₂:Mn⁵⁺ (M = V, P) Nanoparticles. *RSC Adv.* **2017**, *7*, 10564–10569. [[CrossRef](#)]
15. Im, W.B.; Fellows, N.N.; DenBaars, S.P.; Seshadri, R.; Kim, Y.-I. LaSr₂AlO₅, a Versatile Host Compound for Ce³⁺-Based Yellow Phosphors: Structural Tuning of Optical Properties and Use in Solid-State White Lighting. *Chem. Mater.* **2009**, *21*, 2957–2966. [[CrossRef](#)]
16. Unithrattil, S.; Kim, H.J.; Im, W.B. Phase Formation and Luminescence Properties of Ternary Solid-Solution among Tetragonal Systems. *J. Alloys Compd.* **2019**, *798*, 635–643. [[CrossRef](#)]
17. García, C.R.; Oliva, J.; Díaz-Torres, L.A. Photocatalytic Activity of LaSr₂AlO₅:Eu Ceramic Powders. *Photochem. Photobiol.* **2015**, *91*, 505–509. [[CrossRef](#)]
18. Rodríguez-García, C.E.; Perea-López, N.; Raymond, O.; Hirata, G.A. Photoluminescence Properties of Eu-Doped LaSr₂AlO₅. *Sci. Adv. Mater.* **2012**, *4*, 563–567. [[CrossRef](#)]
19. Gu, X.; Fu, R.; Jiang, W.; Zhang, P.; Tang, Y.; Coşgun, A. Photoluminescence Properties of an Orange-Red LaSr₂AlO₅:Sm³⁺ Phosphor Prepared by the Pechini-Type Sol-Gel Process. *J. Rare Earths* **2015**, *33*, 954–960. [[CrossRef](#)]
20. Oliva, J.; García, C.R.; Díaz Torres, L.A.; Camacho, C.; Guzman-Rocha, M.; Romero, M.T.; Hirata, G.A. Effect of the Er³⁺ Co-Dopant on the Green Upconversion Emission of LaSr₂AlO₅:Yb³⁺ Phosphors. *J. Electron. Mater.* **2018**, *47*, 6567–6574. [[CrossRef](#)]
21. Izumi, F.; Momma, K. Three-Dimensional Visualization in Powder Diffraction. *Solid State Phenom.* **2007**, *130*, 15–20. [[CrossRef](#)]
22. Zhao, M.; Han, A.; Ye, M.; Wu, T. Preparation and Characterization of Fe³⁺ Doped Y₂Ce₂O₇ Pigments with High near-Infrared Reflectance. *Sol. Energy* **2013**, *97*, 350–355. [[CrossRef](#)]
23. Thieme, C.; Rüssel, C. Temperature Resistant Red and Purple Ceramic Pigments Based on the Solid Solution Series BaZn_{2-x}Ni_xSi₂O₇ and BaMg_{2-x}Ni_xSi₂O₇. *Dyes Pigment.* **2014**, *111*, 75–80. [[CrossRef](#)]
24. Saraswathy, D.; Prabhakar Rao, P.; Raj, A.K.V.; Ajuthara, T.R. Enhanced Pigmentary Properties of Rare Earth Germanates of the Type La₂CuGe₂O₈ through CuO₆ Octahedron Distortion. *Dyes Pigment.* **2017**, *142*, 472–480. [[CrossRef](#)]
25. Meseguer, S.; Tena, M.A.; Gargori, C.; Galindo, R.; Badenes, J.A.; Llusar, M.; Monrós, G. Development of Blue Ceramic Dyes from Cobalt Phosphates. *Ceram. Int.* **2008**, *34*, 1431–1438. [[CrossRef](#)]
26. Kuleshov, N.V.; Mikhailov, V.P.; Scherbitsky, V.G.; Prokoshin, P.V.; Yumashev, K.V. Absorption and Luminescence of Tetrahedral Co²⁺ Ion in MgAl₂O₄. *J. Lumin.* **1993**, *55*, 265–269. [[CrossRef](#)]

27. Shannon, R.D. Revised Effective Ionic Radii and Systematic Studies of Interatomic Distances in Halides and Chalcogenides. *Acta Cryst.* **1976**, *32*, 751–767. [[CrossRef](#)]
28. Llusar, M.; Forés, A.; Badenes, J.A.; Calbo, J.; Tena, M.A.; Monrós, G. Colour Analysis of Some Cobalt-Based Blue Pigments. *J. Eur. Ceram. Soc.* **2001**, *21*, 1121–1130. [[CrossRef](#)]
29. Gaudon, M.; Robertson, L.C.; Lataste, E.; Duttine, M.; Ménétrier, M.; Demourgues, A. Cobalt and Nickel Aluminate Spinel: Blue and Cyan Pigments. *Ceram. Int.* **2014**, *40*, 5201–5207. [[CrossRef](#)]
30. Momma, K.; Izumi, F. VESTA 3 for Three-Dimensional Visualization of Crystal, Volumetric and Morphology Data. *J. Appl. Crystallogr.* **2011**, *44*, 1272–1276. [[CrossRef](#)]

Disclaimer/Publisher’s Note: The statements, opinions and data contained in all publications are solely those of the individual author(s) and contributor(s) and not of MDPI and/or the editor(s). MDPI and/or the editor(s) disclaim responsibility for any injury to people or property resulting from any ideas, methods, instructions or products referred to in the content.